Incorporation of Al2O3 into cellulose triacetate membranes to enhance the performance of pervaporation for desalination of hypersaline solutions

by Indah Prihatiningtyas

Submission date: 17-Mar-2022 11:45AM (UTC+0700)
Submission ID: 1786137300
File name: Al2O3_Desalination.pdf (2.09M)
Word count: 7873
Character count: 41101

Desalination 474 (2020) 114198

Contents lists available at ScienceDirect

Desalination

journal homepage: www.elsevier.com/locate/desal

Incorporation of Al_2O_3 into cellulose triacetate membranes to enhance the performance of pervaporation for desalination of hypersaline solutions

Indah Prihatiningtyas[a,b,*,1], Gebrehiwet Abrham Gebreslase[a,c,1], Bart Van der Bruggen[a,d,*]

[a] Department of Chemical Engineering, KU Leuven, Celestijnenlaan 200F, B-3001 Leuven, Belgium
[b] Department of Chemical Engineering, Mulawarman University, Jalan Sambaliung No. 9, Sempaja Selatan, Samarinda, Kalimantan Timur, Indonesia
[c] Department of Chemical Engineering, Mekelle Institute of Technology, Mekelle University, P.BOx 1632, Aynalem, Mekelle, Ethiopia
[d] Faculty of Engineering and the Built Environment, Tshwane University of Technology, Private Bag X680, Pretoria 0001, South Africa

ARTICLE INFO

Keywords:
Al_2O_3
Cellulose triacetate
Nanocomposite membrane
Pervaporation
Desalination

ABSTRACT

In this study, nanocomposite membranes were prepared by incorporating alumina (Al_2O_3) nanoparticles into cellulose triacetate (CTA) membranes in order to enhance the performance of pervaporative desalination. The resulting membranes were characterized by SEM, TGA, water contact angle, water uptake, tensile strength, and FTIR. The desalination performance was investigated as a function of Al_2O_3 loading, feed temperature (ranging from 40 to 70 °C) and feed concentration (varying from 0 g/L to 90 g/L NaCl). Pervaporation (PV) experiments showed that incorporating 2% Al_2O_3 into a CTA membrane increased the water flux by 204% compared to pristine CTA (from 2.2 $kg\,m^{-2}\,h^{-1}$ to 6.7 $kg\,m^{-2}\,h^{-1}$) for a 30 g/L NaCl feed solution at 70 °C, while the salt rejection remained above 99.8%. Moreover, when the CTA-2% Al_2O_3 nanocomposite membrane was tested with a 90 g/L feed solution, only 25% flux reduction without sacrificing the salt rejection. Furthermore, different feed concentration affected the activation energy of water molecules to diffuse through pristine CTA and CTA/Al_2O_3 nanocomposite membrane. However, the nanocomposite membrane has a lower apparent activation energy even at high NaCl concentrations, compared to the pristine CTA. This suggests that the developed CTA/Al_2O_3 nanocomposite membrane is suitable for desalting hypersaline water.

1. Introduction

The rise in population growth, economic development, climate change, increasing industrialization and agricultural activities lead to an increase in the fresh water demand. Less than 0.5% of the earth's total water reserves are fresh water; however, obtainable fresh water from rivers and groundwater are currently limited and are being gradually diminished in many places due to water pollution. In contrast, about 97% is seawater [1] which cannot be used directly for human daily needs, industrial and agricultural usages. Desalination converts salty water to fresh water from the almost unlimited supply of seawater. Desalination technologies include thermal desalination, membrane processes, chemical processes, and adsorption [2–4]. Multi stage flash (MSF), multi-effect distillation (MED) and reverse osmosis (RO) are commercial technologies for desalination. However, a process with lower cost would allow for more massive scale applications; furthermore, desalination has environmental impacts, which should be remediated. Currently, membrane technology by RO is interesting for desalination due to its advantages, such as its high efficiency and potential energy saving compared to thermal desalination [5,6], high operational stability, low chemical expenses, easy integration and control within industrial processes [6]. RO is an established membrane technology for desalination since nearly 60% of the installed capacity in the world is operated by RO [7,8]. However, RO requires a high operating pressure to overcome the osmotic pressure, especially when the feed salt concentration is high. Besides, it needs extensive feed pretreatment before being subjected to the membrane to prevent scaling/fouling. Hence, membrane fouling is another impediment [9–11].

Pervaporation (PV) is a membrane process with growing interest as a potential alternative for desalination; it may be preferred over other technologies such as RO due to its potential for desalting hypersaline water [12] and its low energy consumption. PV allows a selective component in the feed solution to penetrate through a dense membrane because of the different solubility and diffusivity of each component in the membrane by solution-diffusion. The driving force is the difference vapor pressure between the feed side and the permeate side of the

* Corresponding authors at: Department of Chemical Engineering, KU Leuven, Celestijnenlaan 200F, B-3001 Leuven, Belgium.
E-mail addresses: indahprihatiningtyas.yamsidi@kuleuven.be (I. Prihatiningtyas), bart.vanderbruggen@kuleuven.be (B. Van der Bruggen).
[1] Authors contributed equally to this work.

https://doi.org/10.1016/j.desal.2019.114198
Received 5 September 2019; Received in revised form 27 October 2019; Accepted 28 October 2019
Available online 02 November 2019
0011-9164/

membrane by an applied vacuum or sweep gas at the permeate side. PV has been applied in the industry for organic solvent dehydration, and to some extent, for the removal of volatile organics from aqueous solutions. PV has been explored for seawater desalination due to its advantages: no need of a higher operating pressure to cope with the osmotic pressure, no extensive pre-treatment of the feed solution, high salt rejection (> 99%), less fouling propensity, and PV is able to handle highly salt concentrated waters [4,13]. However, the main challenge of PV desalination is the low water flux compared to RO.

Many researchers employed polymeric and inorganic materials for pervaporation desalination: polyether amide [14], de-acetylated cellulose acetate [15], cellulose triacetate [12], poly(vinyl-alcohol)/maleic-anhydride/silica [16], cottoncellulose [17], clinoptilolite-phosphate [18], sulfonated polyethylene hollow fibers [19], NaA zeolite [20], polyether ester [21]. All these membranes showed an outstanding salt rejection performance, but the water flux is low, which hampers PV desalination for practical application. Besides, the low tensile strength and the instability during long time operation for hot feed solutions because of the super hydrophilicity is also another challenge. Cellulose triacetate (CTA) is one of cellulose based material which is abundantly available at low cost. CTA is attractive polymeric materials for desalination application because it has an outstanding salt rejection potential, moderate mechanical strength, relatively low cost, improved oxidant resistance, less fouling propensity and can be produced as a dense film [22–24].

There are certain strategies to enhance the water flux: increasing the membrane hydrophilicity, reducing the mass transfer resistance of the membrane, reducing the membrane thickness [4]. In addition, the researchers also need to pay attention in developing membrane materials for PV desalination, which it will be attractive and feasible if the production costs of the PV membranes for desalination are low. In recent years, nanocomposite membranes composed of a polymer and inorganic or organic nanoparticles have been developed for microfiltration, ultrafiltration, nanofiltration, reverse osmosis and pervaporation. Embedding hydrophilic inorganic nanofillers into the matrix of organic materials to develop a composite membrane potentially improves the productivity, selectivity and thermochemical durability of a membrane [25]. Some of the nanoparticles reported include TiO_2[49], SiO_2[47,48], Al_2O_3[30], graphene oxide (GO) [26,27], carbon nanotubes [28] and cellulose nanocrystals (CNCs) [29]. Al_2O_3 nanoparticles attract attention due to their interesting chemical and physical properties; they have a high surface area and a high hydrophilicity [31].

In this study, nanocomposite PV membranes consisting of CTA polymer incorporated with Al_2O_3 nanoparticles were developed by phase inversion-solvent evaporation method. Al_2O_3 nanoparticles incorporated into the polymer matrix yields a composite membrane with stable and attractive separation performance. To the best of our knowledge, there is no published study on CTA/Al_2O_3 nanocomposite membranes employed for pervaporative desalination. Instead, the effect of CTA/Al_2O_3 nanocomposite membrane on the desalination PV performance was investigated in this paper. A series of nanocomposite CTA/Al_2O_3 membranes was characterized in terms of water flux and salt rejection and the results showed that the developed CTA/Al_2O_3 nanocomposite membrane is a potential for desalting hypersaline water compared to pristine CTA membrane.

2. Experimental

2.1. Materials

Cellulose triacetate (CTA, acetyl content 43–44%, molecular weight 966.845 g/mol, Across Organics TM) was used as the base polymer. Aluminum oxide nanoparticles (Al_2O_3, with particle size ≤ 20 nm and specific surface area ≤ 200 m^2/g) purchased from Aladdin were used as fillers. Dimethyl sulfoxide (DMSO, 99% pure) purchased from Fisher Scientific U.K, Ltd., was used as a solvent due to its relatively minimal toxicity; DMSO was reported as a green solvent [32,33]. Sodium chloride with analytical reagent grade (NaCl, ≥99.5%) was acquired from Fisher Scientific U.K, Ltd. All reagents were used as received without any further modification/purification.

2.2. Membrane preparation

Pristine CTA membranes were prepared by dissolving 8 wt% of solid CTA polymer in DMSO. A homogeneous casting solution was obtained by stirring the mixture at 80 °C overnight. The solution was allowed to stand in a fume hood for 12 h to remove air bubbles formed during the stirring. The dope solution was casted onto clean glass plates at room temperature and a relative humidity of 35% with casting height of 200 μm and a casting speed of 0.09 cm/s. The casted polymer film was immediately placed in a vacuum oven set at 60 °C for 4 h to evaporate the solvent. Finally, the membranes were detached from the glass plate by immersing the dried membranes into a water bath.

CTA/Al_2O_3 nanocomposite membranes were fabricated by dispersing different weight percentages of Al_2O_3 (1, 2, 3 and 4 wt%) in DMSO. This mixture was then stirred overnight at 80 °C and sonicated for 1 h. Subsequently, 8 wt% of CTA solid polymer was added to the suspension of Al_2O_3 and stirred overnight. The dope solution was then sonicated for 1 h and was left for another 12 h to remove air bubbles. The dope solution mixture was then casted in the same manner to prepare pristine CTA membranes.

2.3. Membrane characterization

2.3.1. Contact angle analysis

A contact angle goniometer Data physics Instruments (Krüss GmbH Germany, model: DSA 10-Mk2) was employed to investigate the hydrophilicity of the membranes at room temperature. The water contact angle of the samples was taken using drop shape analyzing software to study the water pendant drops. Milli-Q water (2 μL) was dropped at a speed of 24.79 μL/min on the membrane surface. The contact angle was measured at six different locations, and the mean value was considered as the final result.

2.3.2. Water uptake analysis

The water uptake of the pristine CTA and CTA/Al_2O_3 nanocomposite membranes was determined by the following procedure; (i) The specimen was dried in an oven at 105 °C for a day (ii) the dried membrane was immersed in milli-Q water at room temperature for two days to reach adsorption equilibrium (iii) then, the wet membrane (Ww) was wiped with a tissue to remove unabsorbed water, and the membrane was instantly weighed (iv) finally, the mass of the dried membrane (Wd) was obtained by drying the membrane in an oven at 105 °C for 24 h and weighing. The water uptake of the membranes was determined according to the following equation.

$$Water\ uptake\ (\%) = \frac{W_w - W_d}{W_d} \times 100\% \quad (1)$$

2.3.3. SEM analysis

A scanning electron microscopy (SEM) (Philips XL30 SEM, the Netherlands) analysis was performed to scrutinize the surface and cross-sectional morphology difference between the pristine CTA and CTA/Al_2O_3 nanocomposite membranes. The samples were fractured in cryogenic liquid nitrogen before observation of the cross-section. Each sample was sputter-coated with a thin layer of gold under vacuum to prompt conductivity before examining. Different kV voltages were used to obtain the images: a voltage of 10 kV for the cross-section SEM images and 5 kV for the membrane surface SEM images.

2.3.4. FTIR analysis

The chemical composition of the pristine CTA and the change of the

chemistry of CTA/Al_2O_3 nanocomposite membrane were investigated by attenuated total reflectance-Fourier transform infrared spectroscopy (ATR-FTIR, Perkin Elmer, spectrum 100, USA). The spectra were in the span of 4000–650 cm^{-1}.

2.3.5. Mechanical analysis

The mechanical properties such as the tensile strength, and Young modulus of the pristine CTA and the CTA/Al_2O_3 nanocomposite membranes were examined using a testing machine (mini tensile/compression machine, Instron 5943) at room temperature and at a speed of 2 mm/min. At least three specimens for each of the different membranes were measured and an average value was considered.

2.3.6. TGA analysis

The thermal stability of the pristine CTA and CTA/Al_2O_3 nanocomposite membranes was investigated by a thermo-gravimetric analyzer (TGA Q 500, TA instruments, USA). The samples (4–5 mg) were placed in the sample pan and heated up to 550 °C at rate of 10 °C/min under nitrogen purge (40 mL/min), then the mass loss was recorded.

2.3.7. Pervaporation experiment

The performance of CTA/Al_2O_3 nanocomposite membranes in desalination by pervaporation was studied in a laboratory scale apparatus. The membrane was placed and sealed in a stainless steel module with an effective membrane area of 19.625 cm^2. During the measurements, milli-Q water and a range of salt concentrations in the feed were used to test the desalination performance of the membranes. A well-mixed and stirred feed solution was poured into the feed tank and heated to the intended operating temperature. The liquid feed was then pumped into the membrane module with a peristaltic pump, at a speed of ± 80 L/h and the retentate was circulated into the feed tank. A vacuum pump with low pressure below 1 mbar was used at the permeate side of the membrane to create the vapor pressure difference across the membrane and the permeate vapor was collected in a cold trap using a double U shaped glass tube immersed in liquid nitrogen. One measurement took at least 2 h and in the interval of time, the collected permeate was weighed. Each membrane was measured at least three times and the arithmetic mean was taken as the final result. The schematic representation of laboratory scale apparatus used for PV desalination is shown in Fig. 1.

The separation performance of membrane in pervaporation desalination was analyzed in terms of water flux, J (kg m^{-2} h^{-1}) and salt rejection, R (%).

$$Water\ flux\ (J) = \frac{m}{(A \times t)} \quad (2)$$

where m is the amount of water collected at the permeate side (kg), A is the effective area of the membrane (m^2) and t is the time taken to collect the permeate (h). The salt rejection was evaluated using Eq. (3), where C_f and Cp are the salinity in the feed and the permeate solution. The salinity of water was determined by Consort model C831. The conductivity meter was calibrated using different salt standard conductivity solution ranging from 0 to 84 mS/cm (see Fig. S1).

$$Rejection\ (\%) = \frac{(Cf - Cp)}{Cf} \times 100\% \quad (3)$$

3. Result and discussion

3.1. Membrane characterization

3.1.1. Morphological characterization

The primary particle size of the Al_2O_3 nanoparticles was below 20 nm (as indicated by the supplier Aladdin, China). However, there was an aggregation of Al_2O_3 nanoparticles in powder form; this might be because of compression of the nanoparticles during packaging. Fig. 2a shows a SEM image of the powder Al_2O_3 nanoparticles, where it can be seen that the actual particle size is in the range 0.087–11 μm (see Fig. S2).

Agglomeration of nanoparticles in the suspension of Al_2O_3 powder nanoparticles might lead to aggregated nanoparticles in the membrane structure, which leads to a reduction of the mechanical strength [34]. As such it will decrease the membrane performance. Dynamic Light Scattering (DLS) was used to investigate the behavior of Al_2O_3 nanoparticles in the suspensions. Fig. 2b shows the particle size distribution of Al_2O_3 nanoparticles at different concentrations in DMSO. As can be observed from Fig. 2b, the primary particles size of Al_2O_3 in the suspensions are 52–54 nm, then the aggregations of nanoparticles occur at diameter 219 nm, 214 nm, 194 nm, and 212 nm, respectively, for Al_2O_3 content of 1%, 2%, 3% and 4%, while the agglomeration reached to a particle diameter of up to 921 nm for a suspension of 1% Al_2O_3 and up to 2009 nm for 4% Al_2O_3 [35]. Thus, a different content of Al_2O_3 in the suspension affected the agglomeration. Theoretically, the inter-particle interaction played a major part in affecting the dispersion behavior of nanoparticle suspension. Neighboring nanoparticles have a tendency to aggregate together, especially within short distances when the attractive forces such as van der Waals dispersion force dominates over the repulsive forces [36]. Increasing the concentration of Al_2O_3 reduces the

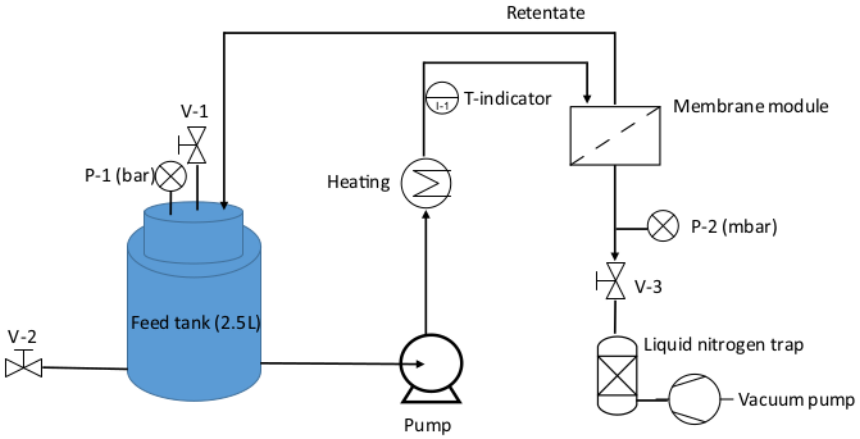

Fig. 1. Schematic laboratory scale apparatus for pervaporation membrane desalination process.

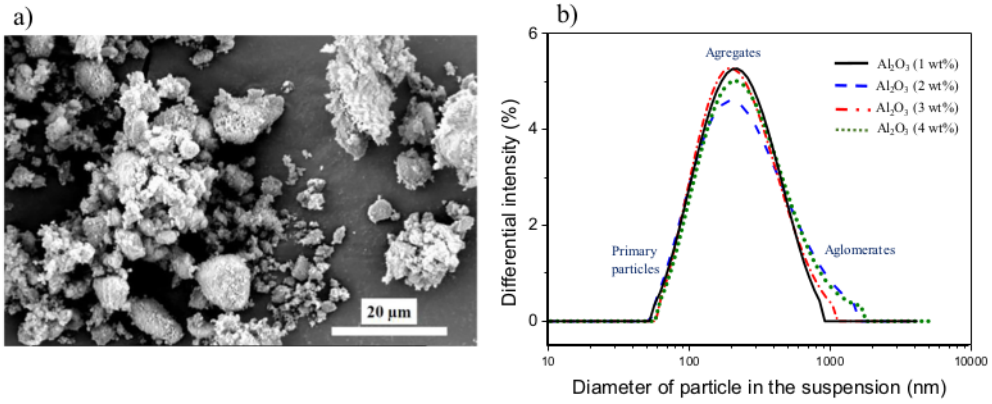

Fig. 2. SEM image of the powder Al_2O_3 nanoparticles (a), and diameter of Al_2O_3 nanoparticles in the suspension (b).

distance between Al_2O_3 nanoparticles, leading to reduced electrostatic repulsion, hence the agglomeration occurs.

An increasing Al_2O_3 content in the suspension also resulted in the enlargement of the average particle size diameter. The effect of increasing nanoparticles on the membrane surface morphology was investigated by SEM images, shown in Fig. 3.

As shown in Fig. 3a, the surface of a pristine CTA membrane was smooth and dense. However, when Al_2O_3 nanoparticles were added to the CTA membrane, the nanoparticles appeared as white spots on the membrane surface (see Fig. 3b–e). Increasing the content of Al_2O_3 nanoparticles up to 4% resulted in numerous protrusions on the membrane surface due to nanoparticle aggregation. Image J was used to measure the length of aggregation of Al_2O_3 nanoparticles based on SEM image (Fig. 3b–e). The smallest and the largest of particle size of aggregation on the membrane surface is listed in Table 1.

The morphology of the cross-section of the membrane was investigated by SEM; the images for pristine CTA and CTA/Al_2O_3 nanocomposite membranes are presented in Fig. 4. Fig. 4a shows an asymmetric membrane with sponge-like structure for pristine CTA, while Al_2O_3 nanoparticles are attached on the sponge-like structure for CTA/Al_2O_3 nanocomposite membranes as shown in Fig. 4b–e. Aggregation of Al_2O_3 nanoparticles also occurs in the cross-section, as can be seen in Fig. 4d–e. SEM images shown in Figs. 3 and 4 reveal that the fabricated membrane are dense, with an asymmetric structure. The images also indicate that increasing the concentration of Al_2O_3 nanoparticles on the CTA membrane results in aggregation of nanoparticles on the surface and in the cross-section of the membrane.

Table 1
Aggregation of Al_2O_3 nanoparticles on the surface of the CTA/Al_2O_3 nanocomposite membrane.

Membrane code	Aggregation of Al_2O_3 (μm)	
	Smallest	Largest
CTA-1% Al_2O_3	0.03	0.65
CTA-2% Al_2O_3	0.10	1.30
CTA-3% Al_2O_3	0.13	3.60
CTA-4% Al_2O_3	0.13	4.19

3.1.2. FTIR characterization

The FTIR analysis of a pristine CTA membrane and CTA/Al_2O_3 nanocomposites membranes is shown in Fig. 5. As expected, all prepared membranes were found to have the typical spectrum of CTA, i.e., a C=O and $-CH_2$ at peak 1737 and 1367 cm^{-1}, C–O stretching and C-O-C at peak 1210 and 1031 cm^{-1}. The characteristic bands at 2955 cm^{-1} and in the range 3631–3484 cm^{-1} are ascribed to the stretching vibration of C–H and O–H, respectively. Compared with the pristine CTA

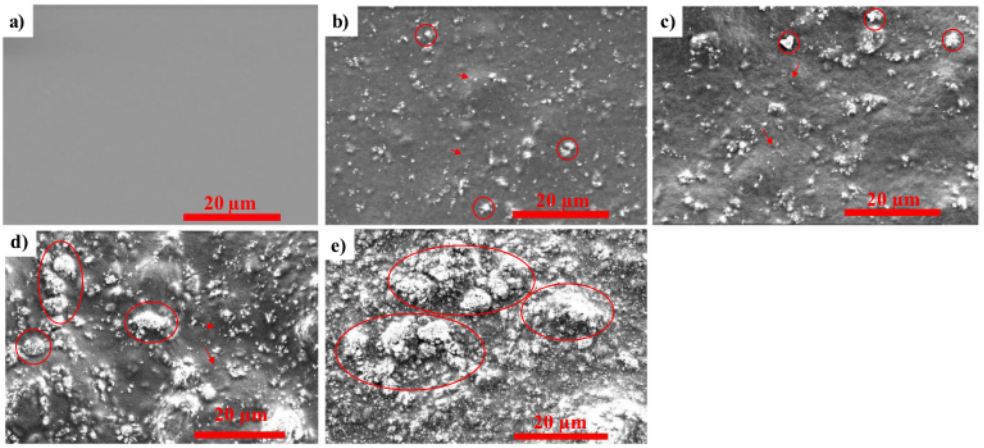

Fig. 3. Top view of SEM images of (a) CTA pristine, (b) CTA-1% Al_2O_3, (c) CTA-2% Al_2O_3, (d) CTA-3% Al_2O_3, and (e) CTA-4% Al_2O_3 nanocomposite membrane (magnification 3500×).

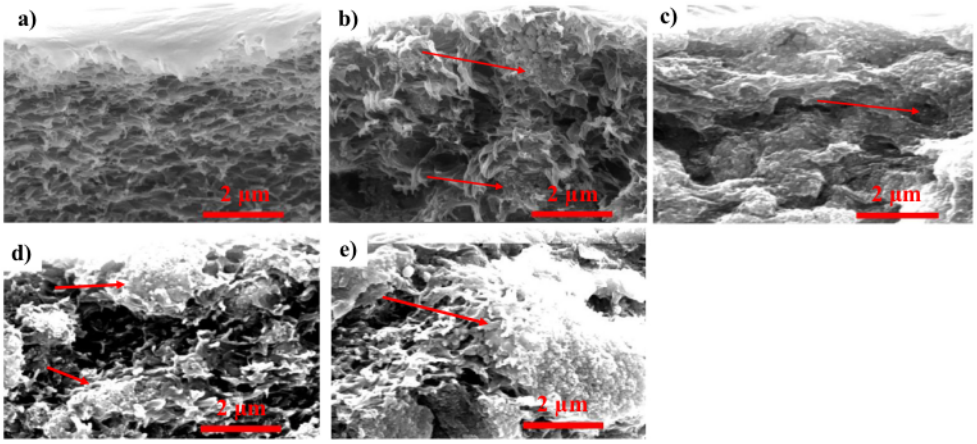

Fig. 4. Cross-sectional of SEM images of (a) Pristine CTA, (b) CTA-1% Al_2O_3, (c) CTA-2% Al_2O_3, (d) CTA-3% Al_2O_3, and (e) CTA-4% Al_2O_3 nanocomposite membrane.

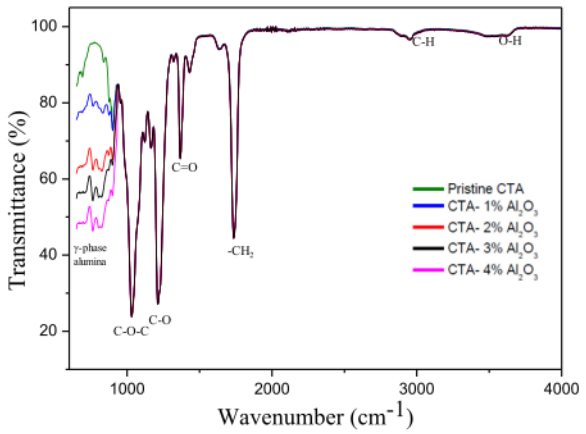

Fig. 5. FTIR spectrum of pristine CTA and CTA/Al_2O_3 nanocomposites membranes.

membrane, new peaks were observed in the range 700–900 cm^{-1}; the peaks in the range 400–1000 cm^{-1} represent the γ-phase of alumina. Fig. 5 shows the asymmetric stretching, symmetric stretching and bending vibrations of the Al–O–Al bonds at 814, 768, and 652 cm^{-1}, respectively [37]. The FTIR results confirm that Al_2O_3 nanoparticles are present in the prepared nanocomposite membranes, while the decreasing percentage of peaks transmittance in the range 700–900 cm^{-1} is related to the higher concentration of Al_2O_3 nanoparticles in the membrane.

3.1.3. Mechanical properties

Tensile strength, Young modulus, and elongation were examined; the results are shown in Fig. 6. In Fig. 6a, it can be seen that the addition of 1% Al_2O_3 resulted in a slight enhancement of mechanical properties compared to the pristine CTA membrane (from 49.5 to 55.96 MPa). However, a further increase up to 4% Al_2O_3 caused a reduction of the tensile strength to 17.32 MPa. This might be due to the presence of aggregated Al_2O_3 nanoparticles on the membrane, as indicated in Table 1, and the non-uniform distribution of Al_2O_3 in the CTA matrix. The aggregation of Al_2O_3 nanoparticles caused by weak adhesion at the interface, thus decreased the tensile strength.

Fig. 6a shows that the incorporation of 1% Al_2O_3 nanoparticles into a CTA membrane improves the tensile strength but the elongation at break decreases. The CTA-1% Al_2O_3 nanocomposite membranes are harder and thus less deformable due to breaks at low strain. Nevertheless, additions of Al_2O_3 nanoparticles of > 2% resulted in a reduction of both of the tensile strength and elongation at break. Increasing the concentration of Al_2O_3 nanoparticles into the CTA dope solution affects the dispersion quality, which leads to weak interactions with the polymer, and subsequently decreases the mechanical properties. Furthermore, the tendency of nanoparticle aggregation occurs at high concentrations of Al_2O_3 in the CTA dope solution, creating macro- and/or microvoids in the membrane, which eventually makes the membrane fragile.

3.1.4. Thermal properties

The thermal behavior of pristine CTA and CTA/Al_2O_3 nanocomposite membranes was studied by TGA analysis. Fig. 7 shows that all the membranes have the similar stage of weight loss. The first stage below 300 °C represents the evaporation of residual moisture or solvent. The second stage in the temperatures range 300 to 380 °C indicates the thermal degradation of the CTA chain and the third is carbonization of the decomposed membranes which occurs at temperatures above 380 °C, leaving the remaining compounds, i.e., inorganic Al_2O_3 nanoparticles. The residual weight loss of the membranes during TGA measurements shows in Fig. S4. It was concluded that the prepared CTA/Al_2O_3 nanocomposite membranes resulted an appropriate thermal stability for PV desalination, which is usually operated in the range of 30–80 °C as feed temperature.

3.1.5. Contact angle and water uptake analysis

The transport mechanism in PV is assumed to be solution-diffusion, in which the first step is adsorption. Hence, a hydrophilic material is important in this process. Generally, contact angle measurement is used to evaluate the surface wettability or hydrophilicity of membrane. The surface hydrophilicity of pristine CTA and CTA/Al_2O_3 nanocomposite membranes was determined by measuring the water contact angle. As presented in Fig. 8a, the pristine CTA membrane has a contact angle of 69°, and the contact angle decreases to 52° with the addition of Al_2O_3 nanoparticles up to 4%. The membrane surface of CTA/Al_2O_3 is more hydrophilic than the pristine CTA due to the greater affinity of metal oxides to water [38]. Increasing the Al_2O_3 nanoparticles content improved the hydrophilicity of the pristine CTA membrane due to the hydrophilicity of the Al_2O_3 nanoparticles, containing hydroxyl groups on the surface. Furthermore, the presence of Al_2O_3 on the membrane

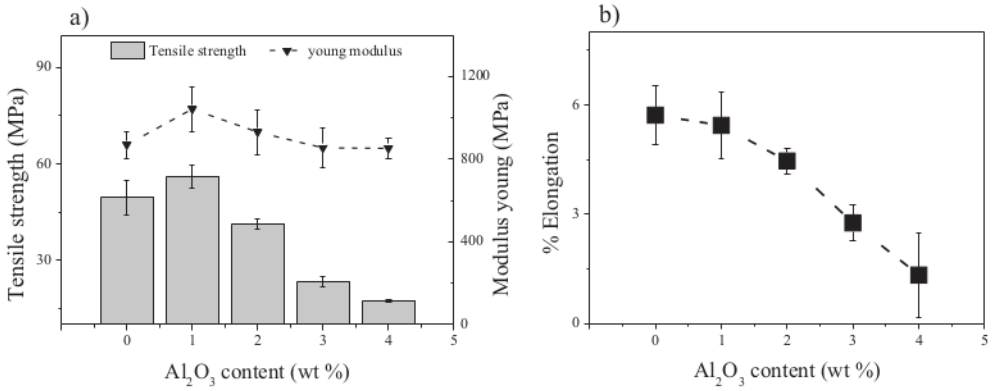

Fig. 6. Mechanical properties of pristine CTA and CTA/Al_2O_3 nanocomposite membranes: a) Tensile strength and modulus young, b) % elongation.

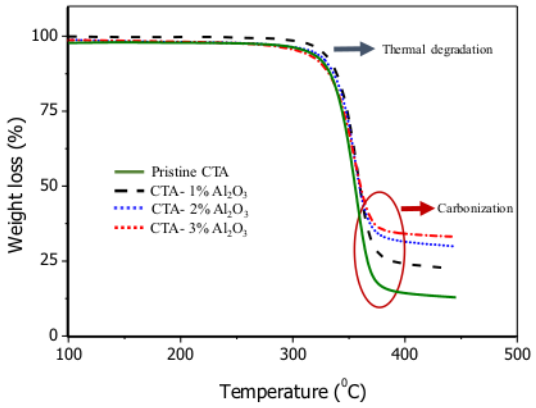

Fig. 7. TGA curve of pristine CTA and CTA/Al_2O_3 nanocomposite membranes.

surface might cause roughness by creating protrusions. The enhancement of the membrane hydrophilicity might potentially accelerate the permeation of water through the membrane.

Water uptake measurements were used to estimate the water adsorption capacity of the membranes. The water uptake of pristine CTA and the nanocomposite membranes is depicted in Fig. 8b. It was found that the water uptake of the membrane increased with the addition of Al_2O_3 nanoparticles in the membrane. The increment of water uptake may be associated with the higher hydrophilicity of the nanocomposite membrane [39]. The maximum water uptake of the nanocomposite membrane was obtained at 2% of Al_2O_3; the water uptake decreased with further addition of nanoparticles due to the aggregation of nanoparticles in the matrix, causing a lower surface area of nanoparticles, which reduces the adsorption of water.

3.2. Performance of CTA/Al_2O_3 nanocomposite membranes in PV desalination

3.2.1. Effect Al_2O_3 content on membrane performance

The effect of the content of Al_2O_3 nanoparticles on the pervaporation desalination performance is indicated in Fig. 9. The water flux of the membrane was substantially elevated with the incorporation of Al_2O_3 nanoparticles. The optimum water flux was obtained with addition of 2% of Al_2O_3 nanoparticles; this flux was three times higher than for the pristine membrane (2.2 $kg\,m^{-2}\,h^{-1}$ to 6.7 $kg\,m^{-2}\,h^{-1}$), while the NaCl rejection remained at 99.8%. The presence of Al_2O_3 nanoparticles in the membrane promoted its hydrophilicity, which eventually enhanced the water flux. However, the water flux diminished with a further increase of Al_2O_3 content. The integration of Al_2O_3 in a CTA membrane improves both the surface hydrophilicity and water uptake (see Fig. 8); nevertheless, a higher content of Al_2O_3 triggers the aggregation of nanoparticles in the polymer matrix (see Figs. 3d–e and 4d–e), which might inhibit the water permeation in the membrane. Furthermore, the thickness of the membrane was increased by increasing the fraction of Al_2O_3 nanoparticles (see Fig. S3). Therefore, the lower water flux may also emanate from the mass transfer resistance as

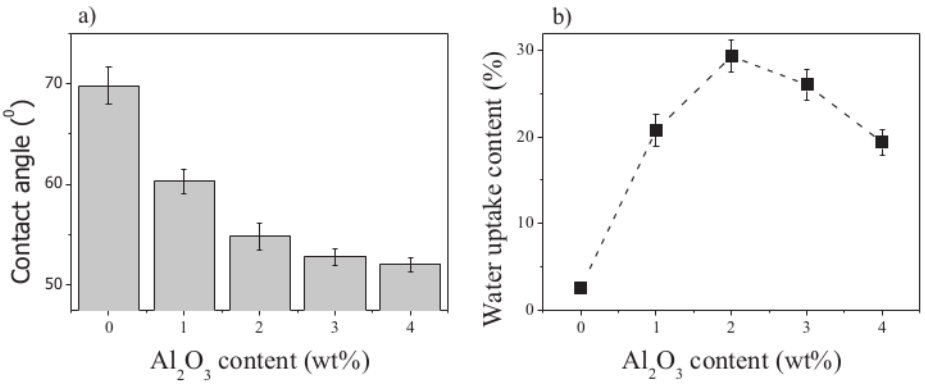

Fig. 8. Contact angle (a), and water uptake (b) of pristine CTA and CTA/Al_2O_3 nanocomposite membranes.

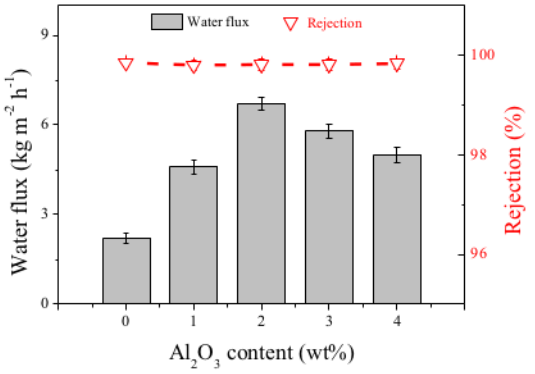

Fig. 9. PV desalination performance at different Al_2O_3 content in the membrane.

the thickness of membrane increases, the mass transfer resistance increases and thus, the water flow through the membrane noticeably declines [29],[40].

Fig. 9 shows the NaCl rejection, which is maintained above 99%. The high rejection in the PV desalination process can be explained as following reasons: 1) NaCl does not permeate to the downstream side of the membrane because it is a non-volatile compound, 2) the major component in the feed is water and CTA/Al_2O_3 is a hydrophilic membrane, so that water molecules will be favorably diffused into the membrane corresponding to the solution-diffusion model [41], 3) All prepared CTA/Al_2O_3 nanocomposite membranes were dense with an asymmetric structure; NaCl does not solubilize in the dense membrane, leading to a high NaCl rejection.

3.2.2. Effect of feed concentration on membrane performance

Fig. 10 shows the effect of the NaCl concentration in the feed on the CTA-2% Al_2O_3 nanocomposite membrane performance at 70 °C. The water flux decreased by 36% for 90 g/L NaCl in the feed solution (7.78 kg m^{-2} h^{-1} to 5 kg m^{-2} h^{-1}), while increasing the NaCl concentration from 30 g/L to 90 g/L reduced the water flux by 25%, from 6.7 kg m^{-2} h^{-1} to 5 kg m^{-2} h^{-1}.

As shown in Fig. 10, the water flux decreases with increasing feed NaCl concentration, while the NaCl rejection is independent of the feed concentration. A higher NaCl concentration in the feed solution decreases the water concentration, which subsequently reduces the sorption of water at the interface of membrane, hence the water flux declines [13]. According to Fick's law, the water flux drops because by

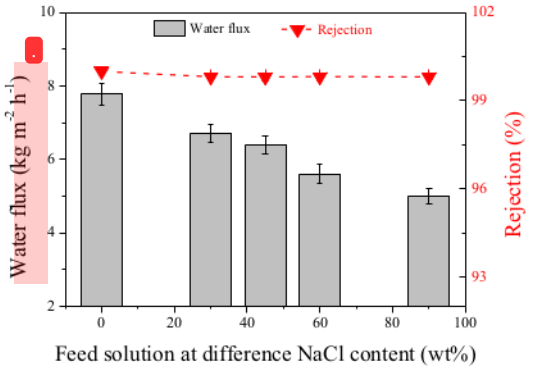

Fig. 10. CTA-2% Al_2O_3 nanocomposite membrane performance at different feed NaCl concentrations at 70 °C.

increasing the salt feed concentration, the thermodynamic activity of water reduces [4]. Increasing the salt concentration in the feed from 30 to 90 g/L corresponds to a decrease of the water concentration from 97 to 91 wt%, and subsequently the sorption of water at the liquid/membrane interface decreases [13], which in turn, negatively affects the driving force of water molecule diffusion through the membrane. Furthermore, at high feed salt concentrations, the concentration of hydrated ions on the membrane surface becomes high; as a result, the water flux declines. The performance of the CTA-2% Al_2O_3 nanocomposite PV membrane was investigated for concentrations in the feed solution in the range of 30–60 g/L, which is around and above the concentration of seawater. When the salt concentration increased to 90 g/L, the water flux decreased by only 25% (5 kg m^{-2} h^{-1}), while the salt rejection remained at least 99.8%. This suggests that the CTA-2% Al_2O_3 nanocomposite PV membrane is suitable for desalination of hypersaline solutions, which can be functional in membrane crystallization in the production of clean water and salt crystals from RO brines, in view of zero liquid discharge.

3.2.3. Effect of feed temperature on membrane performance

Temperature is an imperative factor for the performance of PV desalination, as increasing the feed temperature influences the solubility and diffusivity of water in the membrane [42]. Fig. 11 shows the water flux at different feed temperatures and feed NaCl concentrations for the CTA-2% Al_2O_3 nanocomposite membrane. It was shown that water flux increased with an increasing the feed temperature from 40 to 70 °C. Enhancing the feed temperature leads to an increased water flux. First, the water vapor pressure on the feed side increases exponentially with the feed temperature, while the vapor pressure on the permeate side remains constant; therefore, the driving force increases and consequently the water flux is enhanced. Secondly, increasing the temperature enhances the diffusion coefficient of water, which helps the water molecules to transport through the membrane easily. Thirdly, the larger free volume of the polymeric membrane at higher feed temperatures facilitates the diffusion of water molecules through the free volume [41].

For further elucidation of the effect of temperature on water permeability through the pristine CTA membrane and CTA/Al_2O_3 nanocomposite membrane, the relationship between feed temperature and water flux was fit with an Arrhenius relationship [43].

$$J_i = J_0 \exp\left(\frac{-Ea}{RT}\right) \quad (4)$$

where J_i is the water flux (kg m^{-2} h^{-1}), J_o is the pre-exponential factor

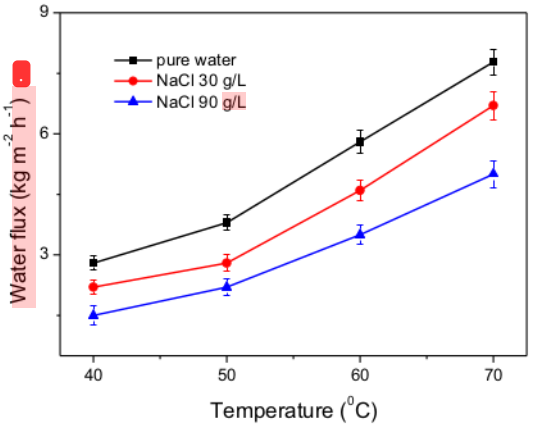

Fig. 11. Water flux at different feed temperatures and NaCl concentrations for a CTA-2% Al_2O_3 nanocomposite membrane.

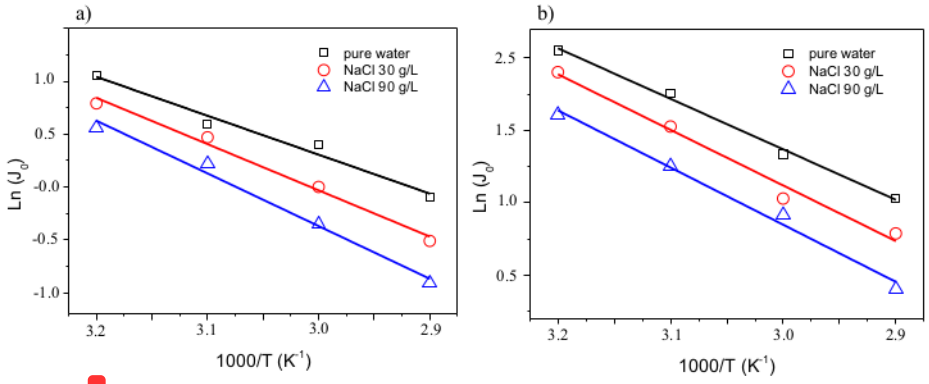

Fig. 12. Arrhenius plot of ln (J) and 1/T: a) Pristine CTA membrane and b) CTA-2% Al_2O_3 nanocomposite membrane.

(kg m^{-2} h^{-1}), R is the gas constant (kJ mol^{-1} K^{-1}), T is the feed temperature (K), and E_a is the activation energy (kJ mol^{-1}), which can be determined from the slope of the Arrhenius plot of ln (J) vs 1/T (Fig. 12).

Fig. 13a shows the Arrhenius plot of ln (J) and 1/T for pristine CTA and Fig. 13b for the CTA-2% Al_2O_3 nanocomposite membrane at different NaCl concentrations. A linear relationship between the natural logarithmic of water flux and the reciprocal temperature was indeed observed.

Table 2 summarizes the activation energy required for water molecules to permeate through the pristine CTA membrane and the CTA-2% Al_2O_3 nanocomposite membrane. It can be seen that the activation energy was increasing with feed concentration for both types of membranes. This might be attributed to the effect of the high mass fraction of salt, leading to concentration polarization, which reduces the water fraction adjacent to the membrane surface, resulting in a pronounced resistance against diffusion and permeation [44]. However, the activation energy for a water molecule to permeate through the CTA-2% Al_2O_3 membranes at different feed concentrations is prominently lower than the activation energy of the pristine CTA membranes. The value of E_a for water permeation through pristine CTA membrane was 43.2 kJ mol^{-1} while for the CTA/Al_2O_3 (2 wt%) nanocomposite membrane it was 34.4 kJ mol^{-1} for a concentration of 90 g/L. The low value of Ea in the CTA-2% Al_2O_3 nanocomposite membrane underlines the enhancement of water permeability through the membrane by the incorporated Al_2O_3 nanoparticles.

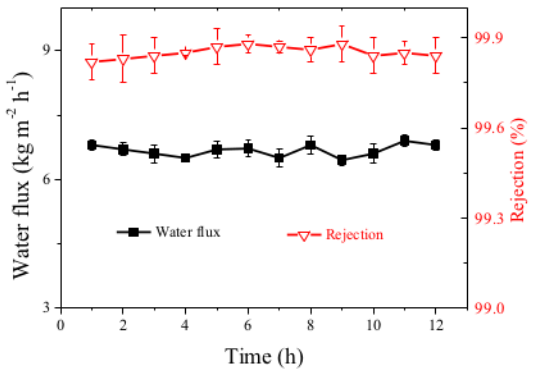

Fig. 13. PV desalination performance of CTA-2% Al_2O_3 nanocomposite during 12 h.

Table 2
Activation energy of CTA and CTA-2% Al_2O_3 nanocomposite membranes in PV desalination at different feed NaCl concentration.

Membrane type	Feed concentration	Activation energy (kJ mol^{-1})
Pristine CTA	Mili-Q water	34.1
	30 g/L NaCl	38.2
	90 g/L NaCl	43.2
CTA-2% Al_2O_3	Mili-Q water	30.8
	30 g/L NaCl	33.3
	90 g/L NaCl	34.4

3.2.4. CTA-2% Al_2O_3 membrane performance in 12 h PV desalination

The CTA-2% Al_2O_3 nanocomposite membrane was investigated for the stability of its performance during 12 h pervaporation. Fig. 13 shows the PV desalination performance of CTA-2% Al_2O_3 nanocomposite during 12 h using a feed solution of 30 g/L NaCl at 70 °C. The water flux was nearly constant and the NaCl rejection was maintained above 99%. Thus, the membrane has a good stability, due to the nature of the dense structure of the membrane, the good compatibility between the fillers and the CTA matrix and the enhanced hydrophilicity of the nanocomposite membrane.

3.2.5. Comparison the pervaporative desalination performance with previous studies

The pervaporative desalination performance of the CTA-Al_2O_3 nanocomposite membrane was compared to other PV membranes for desalination, as shown in Table 3.

The CTA/Al_2O_3 nanocomposite membrane showed better performance than those cellulose based membrane in previous study. However, Xu et al. [26] obtained a higher permeate flux using Graphine oxide/αAl$_2$O in higher temperature with thinness membrane.

4. Conclusion

A series of CTA/Al_2O_3 nanocomposite membranes was prepared using the phase inversion-solvent evaporation method for pervaporation desalination. Blending 2% Al_2O_3 into a CTA casting dope was found to enhance the water flux. The incorporation of Al_2O_3 in CTA membranes improved the hydrophilicity, mechanical strength and thermal stability of the membranes. The water flux of the CTA-2% Al_2O_3 nanocomposite membrane was increased by 204% compared to a pristine CTA membrane (from 2.2 kg m^{-2} h^{-1} to 6.7 kg m^{-2} h^{-1}) using 30 g/L aqueous NaCl as feed solution at 70 °C, with a salt rejection of at least 99.8%. The activation energy required for a water molecule to diffuse through the pristine CTA membrane was increased from 34.1 to 43.2 kJ mol^{-1} using Milli-Q water and 90 g/L of aqueous NaCl solution,

Table 3
List of pervaporation membranes and their performance for desalination.

Membrane	Temperature in feed side (°C)	Conditions on permeate side	Saline feed concentration (g/L)	Membrane thickness (μm)	Flux (kg/m^2.h)	Salt rejection (%)	Reference
Cotton cellulose	40	Vacuum	40	30	4.55–6.7	–	45
Cellulose diacetate on PTFE	40	Vacuum	40	3.5	4.5–5.1	–	45
Cellulose triacetate	50	Air sweep	100	10	2.3	99	12
Cellulose acetate	70	Vacuum	40–140	20–25	5.97–3.45	99.7	44
Graphine oxide/αAl_2O_3	90	Vacuum	35	0.4	48.8	99.7	26
Carbon molecular sieve/ αAl_2O_3	75	Vacuum	35	–	25	93	46
Cellulose triacetate/Al_2O_3	70	Vacuum	30	13	6.7	99.8	This study

respectively; for the CTA-2% Al_2O_3 nanocomposite membrane the activation energy slightly increased from 30.8 to 34.4 kJ mol^{-1}. These results reveal that the CTA-2% Al_2O_3 nanocomposite membrane is suitable for desalting hypersaline water. Moreover, the CTA-2% Al_2O_3 nanocomposite membrane has a good stability of PV desalination performance for 12 h separation. Hence, the CTA/Al_2O_3 nanocomposite membrane is a promising candidate to treat high salinity water for PV membrane application.

Declaration of competing interest

The authors declare there are no competing interests.

Acknowledgment

This research was supported by the Indonesia Endowment Fund for Education (LPDP) and the scholarship of the European Commission - Education, Audiovisual and Culture Executive Agency (EACEA), under the program: Erasmus Mundus Master in Membrane Engineering for sustainable world (EM3E-4SW) (FPA No.20162058, Edition II, http://em3e-4sw.eu/em3e/index.php). The authors would like to thank to Yusak Hartanto for the fruitful discussions (KU Leuven) and Nico Coenen (KU Leuven) for measuring TGA.

Appendix A. Supplementary data

Supplementary data to this article can be found online at https://doi.org/10.1016/j.desal.2019.114198.

References

[1] E. Hameeteman, Future water (in) security: facts, figures, and predictions future water (in) security: facts, figures, and predictions, Glob. Water Inst. (2013) 16.
[2] B. Van der Bruggen, Desalination by distillation and by reverse osmosis — trends towards the future, Membr. Technol. 2003 (2) (2003) 6–9.
[3] P.G. Youssef, R.K. Al-Dadah, S.M. Mahmoud, Comparative analysis of desalination technologies, Energy Procedia 61 (2014) 2604–2607.
[4] Q. Wang, N. Li, B. Bolto, M. Hoang, Z. Xie, Desalination by pervaporation: a review, Desalination 387 (2016) 46–60.
[5] R. Semiat, Critical review energy issues in desalination processes, Environ. Sci. Technol. 42 (22) (2008) 8193–8201.
[6] E. Drioli, A.I. Stankiewicz, F. Macedonio, Membrane engineering in process intensification-an overview, J. Membr. Sci. 380 (2011) 1–2, 1–8.
[7] L. García-Rodríguez, Renewable energy applications in desalination: state of the art, Sol. Energy 75 (5) (2003) 381–393.
[8] C. Charcosset, A review of membrane processes and renewable energies for desalination, Desalination 245 (1) (2009) 214–231.
[9] B. Mayor, Growth patterns in mature desalination technologies and analogies with the energy field, Desalination 2019 (457) (2018) 75–84 May.
[10] A.D. Khawaji, I.K. Kutubkhanah, J.M. Wie, Advances in seawater desalination technologies, Desalination 221 (1–3) (2008) 47–69.
[11] L.F. Greenlee, D.F. Lawler, B.D. Freeman, B. Marrot, P. Moulin, Reverse osmosis desalination: water sources, technology, and today's challenges, Water Res. 43 (9) (2009) 2317–2348.
[12] E. Huth, S. Muthu, L. Ruff, J.A. Brant, Feasibility assessment of pervaporation for desalinating high-salinity brines, J. Water Reuse Desalin. 4 (2) (2014) 109.
[13] D. Wu, A. Gao, H. Zhao, X. Feng, Pervaporative desalination of high-salinity water, Chem. Eng. Res. Des. 136 (2018) 154–164.
[14] H.J. Zwijnenberg, G.H. Koops, M. Wessling, Solar driven membrane pervaporation for desalination processes, J. Membr. Sci. 250 (1–2) (2005) 235–246.
[15] M.M. Elewa, A.A. El-Shafei, A.A. Moneer, M.M. Naim, Effect of cell hydrodynamics in desalination of saline water by sweeping air pervaporation technique using innovated membrane, Desalin. Water Treat. 57 (48–49) (2016) 23293–23307.
[16] Z. Xie, D. Ng, M. Hoang, J. Zhang, S. Gray, Study of hybrid PVA/MA/TEOS pervaporation membrane and evaluation of energy requirement for desalination by pervaporation, Int. J. Environ. Res. Public Health 15 (9) (2018).
[17] Y.P. Kuznetsov, E.V. Kruchinina, Y.G. Baklagina, A.K. Khripunov, O.A. Tulupova, Deep desalination of water by evaporation through polymeric membranes, Russ. J. Appl. Chem. 80 (5) (2007) 790–798.
[18] W. An, X. Zhou, X. Liu, P.W. Chai, T. Kuznicki, S.M. Kuznicki, Natural zeolite clinoptilolite-phosphate composite membranes for water desalination by pervaporation, J. Membr. Sci. 470 (2014) 431–438.
[19] E. Korin, I. Ladizhensky, E. Korngold, Hydrophilic hollow fiber membranes for water desalination by the pervaporation method, Chem. Eng. Process. Process Intensif. 35 (6) (1996) 451–457.
[20] C.H. Cho, K.Y. Oh, S.K. Kim, J.G. Yeo, P. Sharma, Pervaporative seawater desalination using NaA zeolite membrane: mechanisms of high water flux and high salt rejection, J. Membr. Sci. 371 (1–2) (2011) 226–238.
[21] E. Quiñones-Bolaños, H. Zhou, R. Soundararajan, L. Otten, Water and solute transport in pervaporation hydrophilic membranes to reclaim contaminated water for micro-irrigation, J. Membr. Sci. 252 (1–2) (2005) 19–28.
[22] X. Chen, J. Xu, J. Lu, B. Shan, C. Gao, Enhanced performance of cellulose triacetate membranes using binary mixed additives for forward osmosis desalination, Desalination 405 (2017) 68–75.
[23] Yu, Y.; Wu, Q. Y.; Liang, H. Q.; Gu, L.; Xu, Z. K. Preparation and characterization of cellulose triacetate membranes via thermally induced phase separation. J. Appl. Polym. Sci. 2017, 134 (6), 1–10.
[24] X. Zhang, Z. Ning, D.K. Wang, J.C. Diniz da Costa, Processing municipal wastewaters by forward osmosis using CTA membrane, J. Membr. Sci. 468 (2014) 269–275.
[25] A. Karkooti, A.Z. Yazdi, P. Chen, M. McGregor, N. Nazemifard, M. Sadrzadeh, Development of advanced nanocomposite membranes using graphene nanoribbons and nanosheets for water treatment, J. Membr. Sci. 560 (April) (2018) 97–107.
[26] K. Xu, B. Feng, C. Zhou, A. Huang, Synthesis of highly stable graphene oxide membranes on polydopamine functionalized supports for seawater desalination, Chem. Eng. Sci. 146 (2016) 159–165.
[27] L. Li, J. Hou, Y. Ye, J. Mansour, Y. Zhang, V. Chen, Suppressing salt transport through composite pervaporation membranes for brine desalination, Appl. Sci. 7 (8) (2017).
[28] J.H. Jhaveri, Z.V.P. Murthy, Nanocomposite membranes, Desalin. Water Treat. 57 (55) (2016) 26803–26819.
[29] I. Prihatiningtyas, A. Volodin, B. Van der Bruggen, 110th anniversary: cellulose nanocrystals as organic nanofillers for cellulose triacetate membranes used for desalination by pervaporation, Ind. Eng. Chem. Res. 58 (2019) 14340–14349.
[30] N. Uzal, N. Ates, S. Saki, Y.E. Bulbul, Y. Chen, Enhanced hydrophilicity and mechanical robustness of polysulfone nanofiber membranes by addition of polyethyleneimine and Al2O3 nanoparticles, Sep. Purif. Technol. 187 (2017) 118–126.
[31] M. Homayoonfal, M.R. Mehrnia, S. Rahmani, Y. Mohades Mojtahedi, Fabrication of alumina/polysulfone nanocomposite membranes with biofouling mitigation approach in membrane bioreactors, J. Ind. Eng. Chem. 22 (2015) 357–367.
[32] M. Zheng, J. Chen, G. Chen, A. Farajtabar, H. Zhao, Solubility modelling and solvent effect for domperidone in twelve green solvents, J. Mol. Liq. 261 (2018) 50–56.
[33] A. Figoli, T. Marino, S. Simone, E. Di Nicolò, X.M. Li, T. He, S. Tornaghi, E. Drioli, Towards non-toxic solvents for membrane preparation: a review, Green Chem. 16 (9) (2014) 4034–4059.
[34] Y. Zare, Study of nanoparticles aggregation/agglomeration in polymer particulate nanocomposites by mechanical properties, Compos. Part A Appl. Sci. Manuf. 84 (2016) 158–164.
[35] Particle Sciences, Drug development services. Particle size distribution and its measurement, Tech. Br. 2 (2009) 1–2.
[36] F. Yu, Y. Chen, X. Liang, J. Xu, C. Lee, Q. Liang, P. Tao, T. Deng, Dispersion stability of thermal nanofluids, Prog. Nat. Sci. Mater. Int. 27 (5) (2017) 531–542.
[37] S. Ali, Nanoscale advances their potential for use as an adsorbent in the removal of methylene blue dye from industrial wastewater, Nanoscale Adv. 1 (2019) 213–218.
[38] N. Maximous, G. Nakhla, W. Wan, K. Wong, Preparation, characterization and

performance of Al2O3/PES membrane for wastewater filtration, J. Membr. Sci. 341 (1–2) (2009) 67–75.
[39] L. Yan, Y.S. Li, C.B. Xiang, S. Xianda, Effect of nano-sized Al2O3-particle addition on PVDF ultrafiltration membrane performance, J. Membr. Sci. 276 (1–2) (2006) 162–167.
[40] B. Liang, K. Pan, L. Li, E.P. Giannelis, B. Cao, High performance hydrophilic pervaporation composite membranes for water desalination, Desalination 347 (2014) 199–206.
[41] Z. Xie, D. Ng, M. Hoang, T. Duong, S. Gray, Separation of aqueous salt solution by pervaporation through hybrid organic-inorganic membrane: effect of operating conditions, Desalination 273 (1) (2011) 220–225.
[42] P. Schaetzel, C. Vauclair, Q.T. Nguyen, R. Bouzerar, A simplified solution-diffusion theory in pervaporation: the total solvent volume fraction model, J. Membr. Sci. 244 (1–2) (2004) 117–127.
[43] Q. Wang, Y. Lu, N. Li, Preparation, characterization and performance of sulfonated poly(styrene-ethylene/butylene-styrene) block copolymer membranes for water desalination by pervaporation, Desalination 390 (2016) 33–46.
[44] M. Naim, M. Elewa, A. El-Shafei, A. Moneer, Desalination of simulated seawater by purge-air pervaporation using an innovative fabricated membrane, Water Sci. Technol. 72 (5) (2015) 785–793.
[45] Y.P. Kuznetsov, E.V. Kruchinina, Y.G. Baklagina, A.K. Khripunov, O.A. Tulupova, Deep desalination of water by evaporation through polymeric membranes, Russ. J. Appl. Chem. 80 (5) (2007) 790–798.
[46] Y. Song, D.K. Wang, G. Birkett, W. Martens, M.C. Duke, S. Smart, J.C. Diniz Da Costa, Mixed matrix carbon molecular sieve and alumina (CMS-Al_2O_3) membranes, Sci. Rep. 6 (July) (2016) 1–10.
[47] M. Zargar, Y. Hartanto, B. Jin, S. Dai, Hollow mesoporous silica nanoparticles: A peculiar structure for thin film nanocomposite membranes, J. Membr. Sci. 519 (2016) 1–10.
[48] M. Zargar, Y. Hartanto, B. Jin, S. Dai, Polyethylenimine modified silica nanoparticles enhance interfacial interactions and desalination performance of thin film nanocomposite membranes, J. Membr. Sci. 541 (2017) 19–28.
[49] M. Safarpour, A. Khataee, V. Vatanpour, Thin film nanocomposite reverse osmosis membrane modified by reduced graphene oxide/TiO_2 with improved desalination performance, J. Membr. Sci. 489 (2015) 43–54.

Incorporation of Al2O3 into cellulose triacetate membranes to enhance the performance of pervaporation for desalination of hypersaline solutions

ORIGINALITY REPORT

20%	0%	21%	0%
SIMILARITY INDEX	INTERNET SOURCES	PUBLICATIONS	STUDENT PAPERS

MATCH ALL SOURCES (ONLY SELECTED SOURCE PRINTED)

11%

★ Indah Prihatiningtyas, Yusak Hartanto, Bart Van der Bruggen. "Ultra-high flux alkali-treated cellulose triacetate/cellulose nanocrystal nanocomposite membrane for pervaporation desalination", Chemical Engineering Science, 2021

Publication

Exclude quotes	On	Exclude matches	< 2%
Exclude bibliography	On		